

Nonmonotonic energy harvesting efficiency in biased exciton chains

S. M. Vlaming, V. A. Malyshev, and J. Knoester

*Centre for Theoretical Physics and Zernike Institute for Advanced Materials,
University of Groningen, Nijenborgh 4, 9747 AG Groningen, The Netherlands*

We theoretically study the efficiency of energy harvesting in linear exciton chains with an energy bias, where the initial excitation is taking place at the high-energy end of the chain and the energy is harvested (trapped) at the other end. The efficiency is characterized by means of the average time for the exciton to be trapped after the initial excitation. The exciton transport is treated as the intraband energy relaxation over the states obtained by numerically diagonalizing the Frenkel Hamiltonian that corresponds to the biased chain. The relevant intraband scattering rates are obtained from a linear exciton-phonon interaction. Numerical solution of the Pauli master equation that describes the relaxation and trapping processes, reveals a complicated interplay of factors that determine the overall harvesting efficiency. Specifically, if the trapping step is slower than or comparable to the intraband relaxation, this efficiency shows a nonmonotonic dependence on the bias: it first increases when introducing a bias, reaches a maximum at an optimal bias value, and then decreases again because of dynamic (Bloch) localization of the exciton states. Effects of on-site (diagonal) disorder, leading to Anderson localization, are addressed as well.

PACS numbers: 71.35.Aa; 73.63.-b; 78.67.-n 81.16.Fg

I. INTRODUCTION

The harvesting of electromagnetic energy, i.e., its absorption, transport to a specific site, and subsequent trapping in an alternative form of energy, is a process of great importance to life on earth. In nature, systems occur that perform these tasks with amazing efficiency. In order to make the entire process unidirectional, a certain downward energy gradient (bias) occurs. An excellent example is the light-harvesting system in purple bacteria, where photons with a wavelength around 800 nm may be absorbed in the B800 ring of the light-harvesting system 2 (LH2). The resulting excitation may be transferred to the lower-energy B850 ring (850 nm), before undergoing transfer to the yet lower-energy LH1 system (875 nm), from where the final transfer to the so-called special pair of the reaction center occurs ("the trap"). Here, the excitation energy is transformed into chemical energy (see Refs. 1 and 2 for a review). All these steps occur rapidly and with extremely high efficiency. It is well-understood by now that the transport in this system is not described by the classical Förster mechanism^{3,4} of incoherent energy transfer. The excitonic nature plays an important role, both for transport inside and between the various subsystems.^{2,5,6,7,8}

Also in man-made nanoscale systems, the injection of energy at some point and its subsequent transport to and collection at another site, is a process of growing interest. Not only is this relevant to artificial light-harvesting systems, but also to electronic and photonic nanodevices. Obviously, it is important to study how the efficiency of the total process can be optimized.

The aim of the present paper is to study theoretically the effect of a downward energy gradient (bias) on the efficiency of energy harvesting in linear chains of strongly coupled two-level units, and thus to investigate how this process may be optimized. In the context of this paper,

we consider harvesting as the total process following initial excitation at the high-energy side of the chain until its trapping at the low-energy side, i.e., it includes both the transport and the trapping processes. We will choose the average trapping time as a measure for the efficiency of the harvesting process.

At first glance, it seems obvious that a downward bias will reduce the harvesting timescale, and thus will increase its efficiency. Indeed, in the Förster limit of incoherent hopping between weakly coupled sites, an energy bias will cause the excitation to diffuse towards the lower energy end of the chain and will generally lead to a higher quantum efficiency for the harvesting process. Experimental realizations of such chains have been studied by Sauer and coworkers;^{9,10} in addition low-generation dendritic systems with an energy bias towards their core have been studied by various groups.^{11,12,13}

In contrast to the weak-coupling case, the effect of a bias is not clear a priori in chains with strong intersite coupling, where in the absence of a bias the excited states are delocalized (excitons) over the entire chain. On the one hand, the bias defines a preference for the excitation to move towards the trap, on the other hand, it leads to dynamic (Bloch) localization of the exciton states,^{14,15} which slows down the transport process. We will show that, as a result of the competition between both effects, a strong bias always decelerates the harvesting process, while for smaller values of the bias, nonmonotonic behavior may arise. We also study the effect of energetic disorder, which causes Anderson localization^{16,17} and thereby also acts toward reducing the transport efficiency.

To model the harvesting process, we will describe the system by a Frenkel exciton Hamiltonian, with site energies that follow a linear energy bias and, superimposed on that, may suffer from random disorder. The initial state is a localized excitation of a single monomer at the high-energy end of the chain, while at each time the rate

of trapping is proportional to the probability that the monomer at the low-energy end of the chain (the trap) is excited. Thus, to get trapped the exciton should either overlap appreciably with the trap or travel over the chain until it does so. The transport is modeled as an intra-band relaxation process, induced by the scattering of the exciton eigenstates on phonons, and described by a Pauli master equation for the exciton populations. We will restrict ourselves to the zero-temperature limit. A study of temperature effects will be presented elsewhere.¹⁸

Possible realizations of our model are molecular aggregates^{19,20} and conjugated polymers^{21,22} subjected to a non-uniform electric field in order to create a bias (Stark effect), molecular photonic wires^{9,10,23} in which a bias is created by chemical synthesis of a series of molecules with different transition energies, linear arrays of metal nanoparticles,^{24,25} and assemblies of semiconductor quantum dots.^{26,27,28} In the latter two examples, a bias may be created by carefully arranging particles of different size. Another possible application of the underlying physics might be the electrical transport through a single DNA molecule;^{29,30,31,32} the source-drain voltage applied to the DNA is usually on the order of a few volts, which is high enough for dynamic localization to occur.

The outline of this paper is as follows. In the next section, we present our model Hamiltonian. The Pauli master equation for the population dynamics as well as the trapping model are introduced in Sec. III. In Sec. IV, we present our numerical results, analyzing first the effect of a bias on the exciton trapping time in disorder-free chains (Sec. IV A). The interplay of diagonal disorder and a bias is unraveled in Sec. IV B. We summarize and make final remarks in Sec. V.

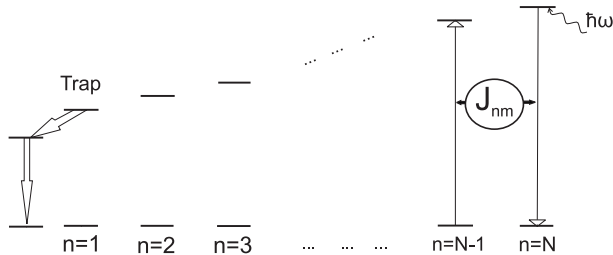


FIG. 1: Schematics of the system under consideration: a one-dimensional array of two-level units with a linearly varying excitation energy. Static disorder can be present as well, introducing an additional stochastic variation in the excitation energies. The initial excitation is created at the high-energy site $n = N$. The excited state of site $n = 1$ is strongly quenched by an additional molecule, so that it acts as a trap.

II. MODEL HAMILTONIAN

We consider a one-dimensional chain of N two-level units with aligned transition dipoles, which are coupled through dipole-dipole transfer interactions. The site excitation energies, in addition to a stochastic component

(diagonal disorder), include a linearly varying part (bias). The schematics of the system is depicted in Fig. 1. The low-energy end of the chain contains a trap, while energy is injected at the high-energy end. In Sec. III, we will define how the transport and trapping processes take place. In this section, we consider the relevant Hamiltonian, which reads

$$H_{ex} = \sum_{n=1}^N [\varepsilon_n + (n-1)\Delta] |n\rangle \langle n| + \sum_{n,m \neq n}^N J_{nm} |n\rangle \langle m|, \quad (1)$$

Here, the state $|n\rangle$ corresponds to site n being excited, while all other sites are in the ground state. The site excitation energy contains two parts: (i) ε_n , which is a Gaussian stochastic variable with mean $\bar{\varepsilon}$ (which can be set to zero without loss of generality) and standard deviation σ , and (ii) the energy bias, characterized by the parameter Δ . The transfer integrals J_{nm} are given by $J_{nm} = -J/|n-m|^3$, with the nearest-neighbor coupling $-J < 0$.

The exciton eigenenergies E_s ($s = 1, \dots, N$) and eigenfunctions $|s\rangle = \sum_{n=1}^N c_{sn} |n\rangle$, with c_{sn} being the n th component of the s th eigenfunction, are found by diagonalizing the matrix $H_{nm} = \langle n| H |m\rangle = \delta_{nm}[\varepsilon_n + (n-1)\Delta] + J_{nm}$ and can be taken real in our model. In the disorder- and bias-free case ($\sigma = \Delta = 0$), the exciton states are delocalized over the whole chain. As a convenient reference case, we note that the wave functions $|s\rangle$ resemble those obtained when only the nearest-neighbor coupling is taken into account.^{33,34,35}

$$|s\rangle = \left(\frac{2}{N+1}\right)^{1/2} \sum_{n=1}^N \sin\left(\frac{\pi sn}{N+1}\right) |n\rangle. \quad (2)$$

The N exciton states form a band with approximate energies

$$E_s = -2J \sum_{n=1}^N \frac{1}{n^3} \cos\left(\frac{\pi sn}{N+1}\right), \quad (3)$$

that range from $E_1 = -2.404J$ to $E_N = 1.803J$, thus having a width $E_N - E_1 = 4.207J$.³³ Note that E_s increases with s ($J > 0$). Throughout this paper (i.e., also in the presence of bias and/or disorder), we will use the convention that s labels the states in order of growing energy. Although Eqs. (2) and (3) are useful for reference, it should be stressed that all results in this paper are obtained by exact numerical diagonalization, accounting for all dipole-dipole interactions.

In a disorder-free system, a nonzero bias results (in the thermodynamic limit $N \rightarrow \infty$) in dynamic (Bloch) localization of all states.^{14,15} The localization size is estimated from semiclassical arguments as $L_B = (E_N - E_1)/\Delta$.³⁶ The Bloch localization is accompanied by the subsequent reorganization of the energy spectrum of the system, which becomes ladder-like with level spacing Δ .³⁷ This structure is revealed in photoluminescence^{38,39} and photoconductivity⁴⁰ spectra of semiconductor superlattices as a series of equally spaced peaks.

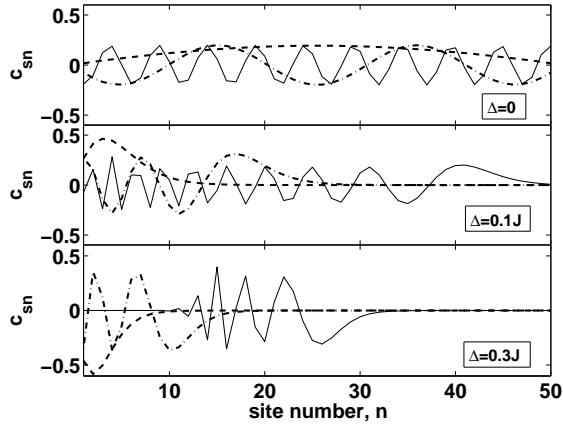


FIG. 2: Exciton wave functions of a disorder-free chain of size $N = 50$ for the states $s = 1$ (dashed curves), $s = 5$ (dash-dotted curves), and $s = 25$ (solid curves) calculated by diagonalizing the Hamiltonian (1) for various magnitudes of the bias: $\Delta = 0$ (upper panel), $\Delta = 0.1J$ (middle panel), and $\Delta = 0.3J$ (lower panel). The lines are a guide for the eye; the coefficients c_{sn} are only defined for integer values of n .

In finite-size systems, dynamic localization comes into play when L_B becomes smaller than the system size N or, in other words, when the overall bias $N\Delta$ exceeds the bare exciton bandwidth $4.207J$. Figure 2, where we plotted several wave functions calculated for three magnitudes of the bias, illustrates this. Note that for $L_B < N$ there exists a strong correlation between the energy of an exciton and its location: the states with smaller s (near the bottom of the exciton band) are localized at the lower energy end of the chain, while the states with higher s (near the top of the band) are localized at the higher energy end. Upon increasing Δ , the bandwidth approaches a value $N\Delta$.⁴¹

Introducing a stochastic component in the site energies ε_n will result in an additional (Anderson) localization effect. At sufficiently high disorder strength σ , the bias-induced correlations between the energy of a state and its location on the chain will be destroyed. The lowest-energy exciton states will not necessarily be located at the low- n side of the chain.

III. TRANSPORT AND TRAPPING MODELS

A. Formalism

The proper description of the dynamics of quantum particles in a system that interacts with a bath, requires the density matrix formalism.^{42,43,44} This holds in particular for the transport and trapping processes underlying the energy harvesting considered here. The system studied is described by the reduced density matrix $\rho_{ss'}$ of the exciton system, which is obtained from the total density operator by tracing out the bath. In our case, the

bath consists of the vibrations in the host surrounding the exciton chain. The diagonal elements ρ_{ss} represent the exciton populations, i.e., the probability that exciton eigenstate s is excited; the $\rho_{ss'}$ for $s \neq s'$ describe the coherences between different exciton states.

For sufficiently weak coupling between the excitons and the host vibrations, we can use the Born-Markov approximation, where it is assumed that the interaction with the host can be treated as a perturbation and that the host is always in equilibrium. A further simplification occurs if we only consider time scales that are long compared to the typical oscillation times of the density matrix elements. This is referred to as the secular approximation,⁴³ and leads to a decoupling of the time evolution of the populations and the coherences.

The time evolution of the populations is then given by the Pauli master equation and does not involve any coherences:

$$\dot{\rho}_{ss} = \sum_{r \neq s} \rho_{rr} W_{sr} - \rho_{ss} \sum_{r \neq s} W_{rs}, \quad (4)$$

where the vibration-induced scattering rates $W_{ss'}$ will be discussed later on. In the secular approximation, the coherences $\rho_{ss'}$ decay exponentially with the dephasing rate $\gamma_{ss'} = \frac{1}{2} \sum_r (W_{rs} + W_{rs'})$ while oscillating in time at a rate $\omega_{ss'} = E_s - E_{s'}$. Additional terms will be included to account for the trap and spontaneous decay and, in fact, the trapping term does introduce a new coupling of the populations to the coherences, as will be seen shortly. However, in most cases we consider, the dephasing of the coherences is sufficiently rapid compared to the harvesting time to allow for a treatment that involves the populations only. A further discussion on the validity of this approach is presented in Sec. III D.

As we already mentioned in the Introduction, the energy harvesting process not only includes the transport, but also the trapping at the low-energy end of the chain. We will assume that the trapping does not affect the exciton wave functions and that this process changes both the exciton populations and coherences with a rate that is proportional to the probability that site $n = 1$ is excited: $\dot{\rho}_{nn'}^{(trap)} = -\frac{1}{2}\Gamma(\delta_{n1} + \delta_{n'1})\rho_{nn'}^{(trap)}$. We will refer to the constant Γ as the quenching or trapping amplitude. By transforming $\dot{\rho}_{nn'}^{(trap)}$ to the exciton basis, it is found that indeed both the exciton populations and coherences are affected by the trap and that the action of the trap couples populations to coherences. If on the timescale of the harvesting the coherences may indeed be neglected, the population of any exciton state s decays nonradiatively with the rate

$$\Gamma_s = \Gamma c_{s1}^2. \quad (5)$$

After accounting for spontaneous emission by introducing a radiative decay channel with rate $\gamma_s = \gamma_0(\sum_n c_{sn})^2$ (γ_0 is the radiative decay rate of an isolated monomer), the overall exciton population dynamics can be described by the following Pauli master equation for the exciton

populations $P_s \equiv \rho_{ss}$:

$$\dot{P}_s = -(\gamma_s + \Gamma_s)P_s + \sum_{s'} (W_{ss'}P_{s'} - W_{s's}P_s) . \quad (6)$$

As the initial condition to Eq. (6), we will assume that the rightmost site $n = N$ is excited at $t = 0$: $\rho_{nn'}(0) = \delta_{nn'}\delta_{nN}$. A transformation to the exciton basis yields $\rho_{ss'}(0) = c_{sN}c_{s'N}$. This corresponds to a normalized initial exciton population distribution given by $P_s(0) = c_{sN}^2$. Furthermore, our initial condition implies that off-diagonal density matrix elements $\rho_{ss'}$ (exciton coherences) are also created; the effect of these coherences on the energy transport may be relevant when their dephasing times are larger than or comparable in magnitude to the typical harvesting times. This is the case for a sufficiently strong quenching amplitude Γ in combination with strongly delocalized exciton states. We come back to this point in Sec. III D.

B. Exciton scattering rates

In the Born-Markov approximation, the scattering rates $W_{ss'}$ which feature in Eq. (4) are equivalent to those obtained using the Fermi golden rule, with the exciton-vibration interaction serving as the perturbation. As stated above, we think of vibrations in the chain's host medium as the ones mainly responsible for the scattering. We will restrict ourselves to one-phonon processes and use a scattering rate from state s' to state s of the form^{45,46,47}

$$W_{ss'} = W_0 S(|E_s - E_{s'}|) \sum_{n=1}^N c_{sn}^2 c_{s'n}^2 \\ \times \begin{cases} n(E_s - E_{s'}), & E_s > E_{s'} , \\ 1 + n(E_{s'} - E_s), & E_s < E_{s'} \end{cases}$$

Here, the prefactor W_0 is a measure of exciton scattering. The spectral density $S(|E_s - E_{s'}|)$ depends on the details of the exciton-vibration coupling as well as on the vibrational density of states. In particular, within the Debye model for the vibrational modes, this factor is given by $S(E_s - E_{s'}) = (|E_s - E_{s'}|/J)^3$ (see, e.g., Ref 47). We use a Debye-like spectral density with an exponential cut-off factor, $S(E_s - E_{s'}) = (|E_s - E_{s'}|/J)^3 \exp(-|E_s - E_{s'}|/\omega_c)$, where ω_c is a cut-off frequency. Similar spectral densities have been successfully used to fit the optical dynamics in photosynthetic antenna complexes.^{44,48,49,50} Note, however, that the results that we will present later on only weakly depend on the particular form of $S(E_s - E_{s'})$.

The term $\sum_{n=1}^N c_{sn}^2 c_{s'n}^2$ in Eq. (7) represents the overlap integral of exciton probabilities for the states s and s' . It depends on both the magnitude of the bias, Δ , and the strength of the disorder, σ . Because of the overlap integral, only hops between neighboring localized states

are efficient. This strongly limits the exciton transport along the chain.

Finally, $n(E) = [\exp(E/T) - 1]^{-1}$ is the occupation number of the vibrational mode with energy E (the Boltzmann constant is set to unity). Due to the presence of the factors $n(E)$ and $1 + n(E)$, the rates $W_{ss'}$ meet the principle of detailed balance: $W_{ss'} = W_{s's} \exp[(E_s - E_{s'})/T]$. Thus, in the absence of decay channels, the eventual exciton distribution is the Boltzmann equilibrium distribution.

C. Harvesting time

The object of our study will be the harvesting time τ which we define as follows. We first introduce the overall survival time of an exciton as the standard expectation value:

$$\bar{\tau} = \int_0^\infty dt t \left\langle - \sum_s \dot{P}_s(t) \right\rangle = \int_0^\infty dt \left\langle \sum_s P_s(t) \right\rangle , \quad (7)$$

where the angular brackets denote the average over disorder realizations. This quantity should be calculated for two situations: with ($\bar{\tau}$) and without (τ_0) the trap. Finally, the exciton harvesting time τ is obtained by extracting the survival time τ_0 with respect to the radiative decay from the overall survival time $\bar{\tau}$, according to the rule:⁵¹

$$\frac{1}{\tau} = \frac{1}{\bar{\tau}} - \frac{1}{\tau_0} . \quad (8)$$

In fact, calculating τ does not require a full solution of the kinetic equation (6). Indeed, its solution reads

$$P_s(t) = \sum_{s'} (e^{-\hat{R}t})_{ss'} P_{s'}(0) , \quad (9)$$

where we have introduced a matrix \hat{R} with elements

$$R_{ss'} = (\gamma_s + \Gamma_s + \sum_{s''} W_{s''s}) \delta_{ss'} - W_{ss'} . \quad (10)$$

Using Eq. (9), the integration over time in Eq. (7) can be performed formally, yielding

$$\bar{\tau} = \left\langle \sum_{s,s'} R_{ss'}^{-1} P_{s'}(0) \right\rangle . \quad (11)$$

Thus, to calculate τ for a particular choice of parameters, one has to invert two $N \times N$ matrices \hat{R} , namely one for the chain with trap and one excluding the trap.

D. Validity of the formalism

Throughout most of this paper, only the exciton populations are considered, which in most cases is an excellent approximation. The limit $\Gamma \gg W_0$, however, highlights

some limitations of our model, which are caused by not taking the coherences $\rho_{ss'}$ into account. In most situations we consider, this is justified, as the coherences $\rho_{ss'}$ decay with a dephasing rate of an order of magnitude of $\sum_r (W_{rs} + W_{rs'})$. This implies that as soon as some relaxation process is involved in reaching the trap, the harvesting process will be slow enough to allow for the neglect of coherences. However, when the quenching amplitude Γ is large and the exciton states are delocalized over the entire chain (i.e., short chains, small bias and small disorder), our model also produces a clearly unphysical artifact, namely the possibility of instantaneous energy transfer from the site $n = N$ to the trap. This can be clearly seen from the quenching term in the Pauli master equation (6): $-\Gamma_s P_s$ is non-zero at $t = 0$ for the initially populated exciton states. This problem is remedied by including coherences in the trapping term, which in turn leads to coupling between different coherences and populations.

We can estimate when the coherences may safely be neglected by requiring that the probability of the initial population distribution undergoing relaxation should be larger than the probability of being directly caught by the trap: $\sum_s (\sum_{s'} W_{s's} c_{sN}^2) \gg \sum_s \Gamma c_{s1}^2 c_{sN}^2$. For the case of no bias and no disorder, we can use the (approximate) explicit expressions for c_{sn} in Eq. (2) to numerically estimate the above inequality. The left hand side, which depends on the form of the scattering rate, numerically evaluates to a N -independent value of approximately $W_0/20$, while the right hand side can be estimated as $\frac{3\Gamma}{2N}$. This estimate shows that our formalism is valid for $\Gamma < NW_0/30$, which for the chain length $N = 50$ and the scattering amplitude $W_0 = 10J$ used later on translates into $\Gamma < 17J$. Note that at larger biases Bloch localization strengthens the validity of our model, as the delocalized exciton states extending from the initially excited monomer to the trap that are required for direct quenching (i.e., with no relaxation involved) become increasingly rare and relaxation will thus be necessary. In that case, the coherences will dephase sufficiently fast to become irrelevant on the total timescale of the harvesting.

In order to get a more quantitative impression of the effect of coherences, we have performed some additional calculations in a crude model where, within the secular limit, coherent effects on the trapping were taken into account by assuming a simple exponential decay of the coherences, while both population and coherence trapping terms were included:

$$\dot{\rho}_{ss}^{(trap)} = -\Gamma c_{s1}^2 \rho_{ss}^{(trap)} - \frac{1}{2} \Gamma c_{s1} \sum_{r \neq s} c_{s'1} (\rho_{ss'} + \rho_{s's}) , \quad (12a)$$

$$\begin{aligned} \dot{\rho}_{ss'} = & -i\omega_{ss'} \rho_{ss'} - \frac{1}{2} \sum_r (W_{rs} + W_{rs'}) \rho_{ss'} \\ & - \frac{1}{2} \Gamma (c_{s1}^2 + c_{s'1}^2) \rho_{ss'} . \end{aligned} \quad (12b)$$

These equations are obtained by disregarding all terms that couple the time evolution of the coherences to other density matrix elements, while the equation for the time evolution of the populations is complete and naturally also includes the phonon scattering and radiative decay terms discussed previously. Although this is not a consistent approach, it does allow for a first impression of the effect of coherences on population decay. As we will see in Sec. IV, the results of this approach confirm the above estimates.

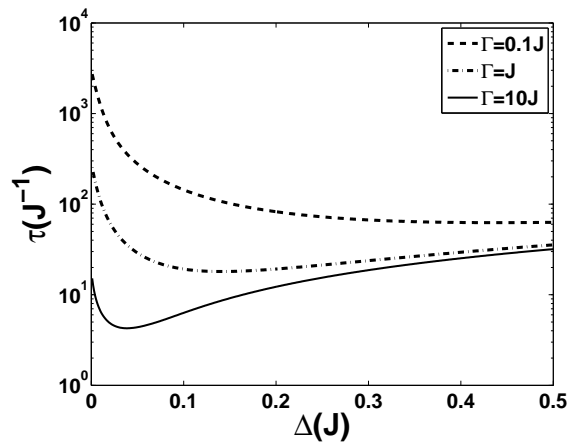


FIG. 3: Harvesting time τ [defined in Eq. (8)] versus the applied bias magnitude Δ calculated for a disorder-free chain of 50 sites for various quenching amplitudes Γ (shown in the plot). The exciton scattering amplitude was set to $W_0 = 10J$.

IV. NUMERICAL RESULTS AND DISCUSSION

All results reported in this paper were obtained by using physical parameters (J , γ_0 , and W_0) typical for a particular physical system where our theory might be applicable, namely molecular aggregates. More specifically, we set $J = 600 \text{ cm}^{-1}$ and $\gamma_0 = 3.6 \times 10^8 \text{ s}^{-1} = 2 \times 10^{-5} J$, which are appropriate values for J-aggregates of the dye pseudocyanine (PIC).^{52,53} The scattering amplitude W_0 was fixed at $W_0 = 10J$, which is consistent with the values found from the fit of the temperature dependence of the J-bandwidth and of the radiative lifetime in J-aggregates of PIC.⁵⁴ The cut-off frequency ω_c of the spectral density $S(E)$ was taken equal to $\omega_c = 0.5J$. The exact value is arbitrary to a large extent and hardly affects the conclusions derived from our study, although it is crucial that some cut-off value is introduced to suppress unphysically energetic phonon modes. To simplify the link to other systems, the nearest-neighbor coupling J was used as the unit for all relevant quantities. We stress once again that all dipole-dipole couplings are taken into account. Chains of size $N = 50$ were considered in all simulations. As was already mentioned in the Introduction, we only consider the zero-temperature limit.

A. Disorder-free biased chain

Figure 3 shows the behavior of the harvesting time τ as a function of the bias magnitude Δ , calculated for a set of quenching amplitudes Γ , indicated in the plot. As is seen, the character of the behavior is strongly affected by Γ , revealing an acceleration of the harvesting process with increasing bias for $\Gamma < W_0 (= 10J)$, while the Δ -dependence at $\Gamma \sim W_0$ is shown to be nonmonotonic. For $\Gamma \gg W_0$, the model predicts a harvesting time that monotonically increases with Δ , starting from $\tau \ll 1/J$ for $\Delta = 0$. We do not show and analyze this limit however, as it describes an unphysically strong quenching effect, with Γ being much larger than the nearest-neighbor coupling J . Such strong quenching would affect the exciton wave functions; moreover, the neglect of coherences is not a valid approximation in this case (cf. Sec. III D).

To unravel the behavior found in Fig. 3, we note that various bias-dependent factors exist that govern the overall energy harvesting process: (i) - the initial distribution of population $P_s(0) = c_{sN}^2$, (ii) - the trapping of the exciton states with rate $\Gamma_s = \Gamma c_{s1}^2$, and (iii) - the intra-band relaxation which populates (or depopulates) the most strongly trapped states. The interplay of all of these factors determines the bias dependence of the exciton harvesting presented in Fig. 3.

We first discuss the initial condition, $P_s(0) = c_{sN}^2$, which in Fig. 4(a) is plotted as a function of the state index s for four choices of the bias strength Δ . In the absence of a bias ($\Delta = 0$), the states in the center of the band are populated to a much larger extent than the states near the bottom and the top of it. Similar behavior occurs in the nearest-neighbor coupling model, where this can be explicitly shown by replacing c_{sN} with the N -th coefficient in Eq. (2). A nonzero bias drastically changes this situation, because of the dynamic localization. The localization dictates that the states which are located near the right-most site $n = N$, i.e. those which have a significant amplitude at the site of initial excitation, are those with higher energies or large s (see Fig. 2). Thus, upon increasing the bias strength, the initial distribution of population will shift to the top of the exciton band. Figure 4(a) clearly illustrates this.

The distribution c_{s1}^2 , which determines the quenching rate Γ_s , shows the opposite tendency, as is seen in Fig. 4(b). In the absence of a bias, it is maximal for the central band states and negligible at the band edges, similar to c_{sN}^2 . Already at a moderate bias, the quenching rate of the states at the bottom of the band increases significantly. For larger bias magnitudes, the distribution c_{s1}^2 strongly shifts to the lower band edge (to small s). For a sufficiently strong bias ($N\Delta > E_N - E_1 = 4.207J$), when the Bloch localization sets in, the initially excited states and those undergoing efficient quenching are separated completely and located at the top and the bottom of the band, respectively.

Finally, an important stage in the harvesting process is the relaxation of excitons from the initially populated

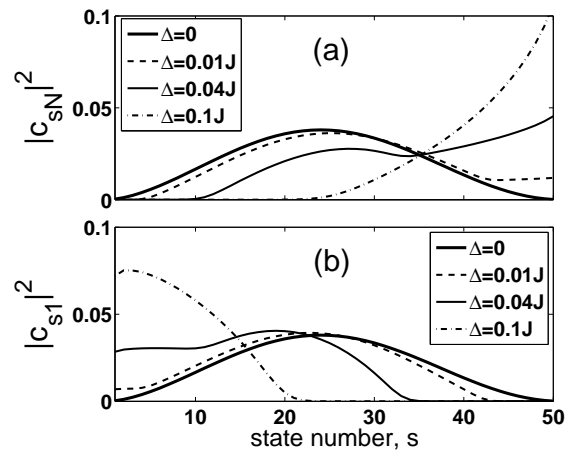


FIG. 4: Bias dependence of the exciton probabilities c_{sN}^2 (a) and c_{s1}^2 (b) that determine the initial distribution of the exciton population $P_s(0)$ and the quenching rate Γ_s , respectively. The bias tends to shift the initial distribution of population to the top of the band (to higher s). Oppositely, the strongly quenched states are shifted to the lower band edge (small s).

states to those where the quenching rates $\Gamma_s = \Gamma c_{s1}^2$ become comparable to or larger than the relaxation rate $\sum_{s'} W_{ss'}$. This relaxation process will generally take longer when increasing the bias magnitude Δ . The reason for this is twofold. First, as we have seen above, for larger bias the excitation and quenching occur at opposite band edges, implying that the excitons have to undergo more relaxation steps to be trapped. Second, the bias-induced localization of the exciton states decreases their probability overlap $\sum_n c_{sn}^2 c_{s'n}^2$, thereby reducing the relaxation rates $W_{ss'}$.

The above observations form the basis for understanding the results in Fig. 3. For small quenching amplitudes, $\Gamma \ll W_0$, the downward relaxation is the fastest process and the trapping step becomes rate-limiting. Eventually, most of the population will end up in the exciton states near the lower band edge, where it waits to be trapped. In the absence of a bias ($\Delta = 0$), these states have negligible quenching rates Γ_s , as explained above, leading to large τ values. After the bias is turned on, the amplitudes of the band edge states at the trapping site $n = 1$ steeply increase, giving rise to a strongly enhanced quenching rate. This will in turn result in a decrease of the overall harvesting time τ . For very large biases, the overall harvesting time will eventually rise again, as a result of the reduced relaxation rates $W_{ss'}$. All this is in agreement with the behavior observed in Fig. 3 for $\Gamma \ll W_0$.

The nonmonotonic Δ -dependence of τ observed in Fig. 3 (reaching a minimal τ value at small bias) occurs when the quenching and scattering amplitudes are comparable, $\Gamma \sim W_0$. This nonmonotonic behavior is caused by the competition between the bias-induced effects discussed above. More specifically, for small but increasing values of Δ , the increase in the quenching rates Γ_s for the exciton states near the bottom of the band

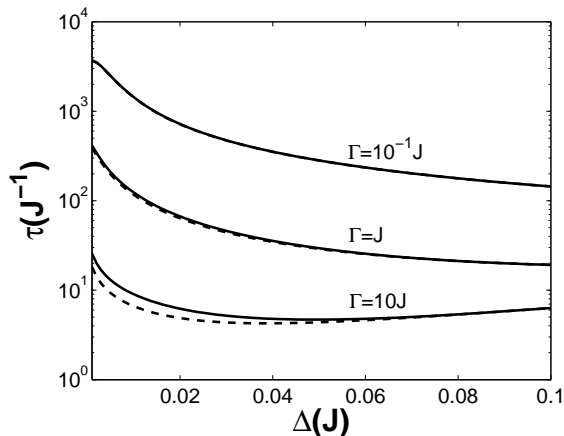


FIG. 5: Harvesting time τ [defined in Eq. (8)] versus the applied bias magnitude Δ calculated for a disorder-free chain of 50 sites. The solid lines correspond to the model where coherences are taken into account, while the dashed lines only account for populations and are identical to the results in Fig. 3.

is the dominant effect. This explains why τ initially decreases as a function of Δ . A further increase in Δ will shift the Γ_s -distribution to the lower band edge, while the $P_s(0)$ -distribution shifts to the upper band edge, making the conditions for quenching less favorable. The connection of these two distributions via the intra-band relaxation accounts for the reduced harvesting efficiency beyond some optimum bias value, due to the decrease of the relaxation rates for increasing Δ . Thus, we conclude that at $\Gamma \sim W_0$, there exists an optimal magnitude of the bias that provides the most efficient harvesting conditions.

It should be noted that for large values of the bias, when the exciton states have become strongly localized, τ becomes independent of the quenching amplitude, because the harvesting process is limited in rate totally by the intraband relaxation. This is confirmed by Fig. 3.

Figure 5 shows the corrections that a crude model (see Sec. III D) for coherent transport yields, where the time evolution of the coherences is assumed to be simply exponential. The corrections are at most somewhere around 25 percent, which makes sense as direct quenching only accounts for a fraction of the total quenched population. Also, dephasing of the coherences is provided through both the exciton-phonon coupling and the trap, and coherent effects are therefore suppressed for all but the fastest energy transfer processes. A full discussion of the effects of coherent transport in unbiased chains should not be limited to the secular treatment provided here, and will be provided in a later paper.

B. Disordered biased chain

In this section, we present a study of the bias-dependent harvesting time τ in disordered chains. We

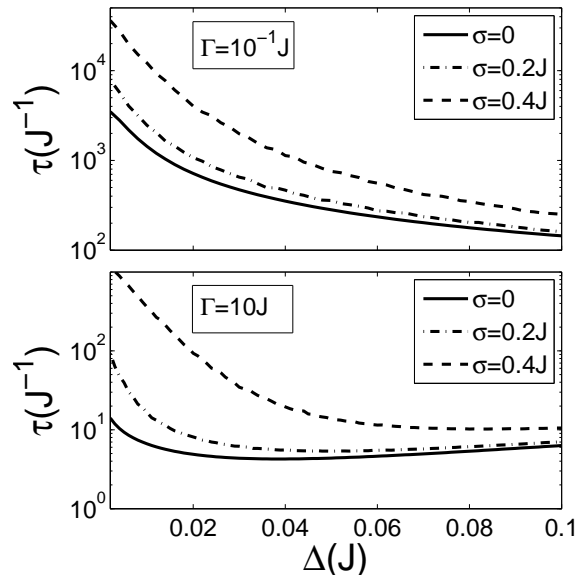


FIG. 6: Effect of uncorrelated on-site Gaussian disorder of strength σ on the bias dependence of the harvesting time τ calculated for two quenching amplitudes $\Gamma = 10^{-1}J$ (upper panel) and $\Gamma = 10J$ (lower panel).

considered on-site Gaussian disorder (uncorrelated for different sites) with zero mean and standard deviation σ , referred to as the disorder strength. Figure 6 shows the results obtained for two quenching amplitudes $\Gamma = 10^{-1}J$ and $\Gamma = 10J$, keeping $W_0 = 10J$ and $N = 50$ in all simulations. For other values of the scattering or quenching amplitude, similar results were obtained. The general observation that can be deduced from Fig. 6 is that the inclusion of disorder leads to a reduced efficiency of the energy harvesting process. The effect is especially significant for small Δ . Another consequence of disorder is that, in the case of $\Gamma \sim W_0$, the magnitude of the bias that is optimal for harvesting shifts to larger values.

The explanation of these observations is straightforward. As we already mentioned, the disorder results in Anderson localization of all the states on segments of the chain. First of all, this localization breaks the correlation that exists at low magnitudes of the bias ($N\Delta \ll E_N - E_1 = 4.207J$) between the distributions $P_s(0)$ and Γ_s : the states that are mostly excited initially and those that are quenched efficiently do not overlap anymore. Secondly, the localized states that have a significant amplitude at the trap are now not necessarily the lowest energy states and can hardly be reached during the downward intra-band relaxation. In addition, the localization slows down the overall exciton relaxation, because of blocking of the diffusion over the localized states at zero temperature.⁵⁵ All these factors result in a reduced harvesting efficiency at zero bias. Higher bias strengths tend to (partially) restore the correlation between the energy and location of an exciton state, in

particular the lowest-energy exciton states will tend to lie in the vicinity of the trap. As a result, the states that are quenched most strongly are more accessible through intraband relaxation. This is why for small bias values Δ , the harvesting time τ always decreases for increasing Δ , independently of the quenching amplitude Γ .

For larger bias magnitudes, such that $N\Delta > E_N - E_1 = 4.207J$, the dynamic localization dominates over the disorder-induced localization. As a consequence, in this region the effect of introducing disorder is very limited, in full agreement with the results presented in Fig. 6. Note that, like the Bloch localization discussed in the previous section and for similar reasons, Anderson localization expands the range of validity of our model.

V. SUMMARY AND CONCLUDING REMARKS

We studied the efficiency of harvesting of excitation energy in chains of strongly coupled dipolar units, in the presence of a linear energy bias. The harvesting combines the excitation transport following initial excitation at one end of the chain and quenching of the excitation by a trap at the other end. The energy gradient was set towards the trap. We considered the quenching rate of a particular exciton state to be proportional to its occupation probability at the position of the trap. Within this model, the energy harvesting efficiency is governed by the interplay of the direct quenching of exciton states due to their overlap with the trap and the exciton relaxation to those states which are quenched most efficiently. We found a complicated scenario for the energy harvesting efficiency as a function of the bias magnitude Δ . Most importantly, we found that a bias does not necessarily increase this efficiency.

The effect of a bias strongly depends on the ratio between the amplitudes Γ (efficiency of the trap) and W_0 (vibration-induced scattering). In the limit of $\Gamma \ll W_0$, the initial population first scatters toward the bottom of the band, where quenching (the slowest process) eventually takes place. Introducing a bias now greatly reduces τ , because of its above mentioned tendency to shift the strongly quenched states to the lower band edge. Sup-

pression of the exciton's downward relaxation upon increasing the bias magnitude now plays a less important role, because the relaxation is not the rate limiting step in the process.

In the intermediate case of $\Gamma \sim W_0$, it depends on the bias strength what is the rate limiting step in the harvesting process. As a consequence, the bias dependence of the harvesting time τ reveals a nonmonotonic behavior, in other words an optimal magnitude of the bias exists at which excitons are harvested most efficiently. As has been explained in Section III, our model is not expected to be appropriate in the limit of $\Gamma \gg W_0$, corresponding to what we expect is an unphysically strong quenching effect, as it does not adequately include coherent effects.

We have also investigated how random energy disorder, superimposed on the overall bias, affects the above findings. We have found that disorder leads to a decrease of the harvesting efficiency, in particular for low bias magnitudes, and gives rise to a nonmonotonic bias dependence of this efficiency, independently of the ratio Γ/W_0 . We have shown that these effects can be understood from the disorder-induced (Anderson) localization of the exciton states. The effects of disorder are smeared at higher bias magnitudes, when the dynamic (Bloch) localization becomes dominant.

To conclude, we note that the competition between the enhancement of transport and quenching, which underlies the interesting nonmonotonic behavior discussed in this paper, is a very common theme in the physics of energy harvesting systems. Although the model presented here is inspired by one-dimensional Frenkel exciton systems, such as J-aggregates and conjugated polymers, it is to be expected that similar effects occur in other physical realizations, such as linear arrays of resonantly coupled quantum dots.

Acknowledgments

This work is supported by NanoNed, a national nanotechnology programme coordinated by the Dutch Ministry of Economic Affairs.

¹ H. Van Amerongen, L. Valkunas, R. van Grondelle, *Photosynthetic Excitons*, World Scientific: Singapore, 2000.
² V. Sundström, T. Pullerits and R. van Grondelle, *J. Phys. Chem. B* **103** 2327 (1999).
³ Th. Förster, *Ann. Phys.* **2**, 55 (1948); in *Modern Quantum Chemistry*, Pt. III, edited by O. Sinanoglu; Academic: New York, 1965.
⁴ V. M. Agranovich and M.D. Galanin, *Electronic Excitation Energy Transfer in Condensed Matter*; North-Holland: Amsterdam, 1982.
⁵ A. M. van Oijen, M. Ketelaars, J. Köhler, T. J. Aartsma, and J. Schmidt, *Science* **285**, 629 (1999).

⁶ H. Sumi, *J. Phys. Chem. B* **103**, 252 (1999).
⁷ K. Mukai, S. Abe, and H. Sumi, *J. Phys. Chem. B* **103**, 6096 (1999).
⁸ S. Jang, M. D. Newton, and R. J. Silbey, *Phys. Rev. Lett.* **92**, 218301 (2004); *J. Phys. Chem. B* **111**, 6807 (2007).
⁹ M. Heilemann, P. Tinnefeld, G. Sanchez Mosteiro, M. Garcia Parajo, N. F. van Hulst, and M. Sauer, *J. Am. Chem. Soc.* **126**, 6514 (2004).
¹⁰ P. Tinnefeld, M. Heilemann, and M. Sauer, *ChemPhysChem* **6**, 217 (2005).
¹¹ C. Devadoss, P. Bharathi, and J. S. Moore, *J. Am. Chem. Soc.* **118**(40), 9635 (1996).

- ¹² D.-L. Jiang and T. Aida, *Nature* **388**, 454 (1997).
- ¹³ R. Kopelman, M. Shortreed, Z.-Y. Shi, W. Tan, Z. Xu, J. S. Moore, A. Bar-Haim, and J. Klafter, *Phys. Rev. Lett.* **78**, 1239 (1997).
- ¹⁴ F. Bloch, *Z. Phys.* **52**, 555 (1927).
- ¹⁵ C. Zener, *Proc. R. Soc. London, Ser. A* **145**, 523 (1934).
- ¹⁶ P. W. Anderson, *Phys. Rev.* **109**, 1492 (1958).
- ¹⁷ E. Abrahams, P. W. Anderson, D. C. Licciardello, and T. V. Ramakrishnan, *Phys. Rev. Lett.* **42**, 673 (1979).
- ¹⁸ S. M. Vlaming, V. A. Malyshev, and J. Knoester, *J. Lumin.* (in press).
- ¹⁹ *J-aggregates*, ed. T. Kobayashi, World Scientific: Singapore, 1996.
- ²⁰ J. Knoester, in *Proceedings of the International School of Physics "Enrico Fermi", Course CXLIX, Organic Nanostructures: Science and Application*, Eds. V. M. Agranovich and G. C. La Rocca (IOS Press, Amsterdam, 2002), pp. 149-186.
- ²¹ A. Tilgner, H.P. Trommsdorff, J.M. Zeigler, and R.M. Hochstrasser, *J. Chem. Phys.* **96**, 781 (1992).
- ²² For a recent overview see, e.g., "Semiconducting Polymers - Chemistry, Physics, and Engineering", eds. G. Hadziioannou and P. van Hutten (VCH, Weinheim, 1999).
- ²³ R. W. Wagner and J. S. Lindsey, *J. Am. Chem. Soc.* **116**, 9759 (1994).
- ²⁴ M. Quinten, A. Leithner, J. R. Kren, and F. R. Aussenegg, *Opt. Lett.* **23**, 1331 (1998).
- ²⁵ D. S. Citrin, *Nano Lett.* **4**, 1561 (2004).
- ²⁶ S. A. Crooker, J. A. Hollingsworth, S. Tretiak, and L. V. Klimov, *Phys. Rev. Lett.* **89**, 186802 (2002).
- ²⁷ T. Franzl, T. A. Klar, S. Schietinger, A. L. Rogach, and J. Feldmann, *Nano Lett.* **4**, 1599 (2004).
- ²⁸ T. A. Klar, T. Franzl, A. L. Rogach, and J. Feldmann, *Adv. Mater.* **17**, 769 (2005).
- ²⁹ D. Porath, A. Bezryadin, S. de Vries, and C. Dekker, *Nature* **403**, 635 (2000).
- ³⁰ B. Xu, P. Zhang, X Li, and N. Tao, *Nano Lett.* **4**, 1105 (2004).
- ³¹ R. Gutiérrez, S. Mandal, and G. Cuniberti, *Nano Lett.* **5**, 1093 (2005); *Phys. Rev. B.* **71**, 235116 (2005).
- ³² A. V. Malyshev, *Phys. Rev. Lett.* **98**, 096801 (2007).
- ³³ H. Fidder, J. Knoester, and D. A. Wiersma, *J. Chem. Phys.* **95**, 7880 (1991).
- ³⁴ V. Malyshev and P. Moreno, *Phys. Rev. B* **51**, 14587 (1995).
- ³⁵ C. Didraga and J. Knoester, *J. Chem. Phys.* **121**, 946 (2004).
- ³⁶ N. W. Ashcroft and N. D. Mermin, *Solid State Physics*, Saunders College Publishers: New York, 1976, p. 213.
- ³⁷ G. H. Wannier, *Phys. Rev.* **117**, 432 (1960).
- ³⁸ E. E. Méndez, F. Agulló-Rueda, and J. M. Hong, *Phys. Rev. Lett.* **60**, 2426 (1988).
- ³⁹ F. Agulló-Rueda, E. E. Méndez, and J. M. Hong, *Phys. Rev. B* **40**, 1357 (1989).
- ⁴⁰ M. K. Saker, D. M. Whitteker, M. S. Skolnick, M. T. Emeny, and C. R. Whitehouse, *Phys. Rev. B* **43**, 4945 (1991).
- ⁴¹ E. Díaz, F. Domínguez-Adame, Yu. A. Kosevich, and V. A. Malyshev, *Phys. Rev. B* **73**, 174210 (2006).
- ⁴² J. von Neumann, *Göttinger Nachrichten* 245 (1927); *Mathematical Foundations of Quantum Mechanics*, (Princeton Univ. Press: New Jersey, 1955).
- ⁴³ K. Blum, *Density Matrix Theory and Applications*, Plenum Press, New York, 1981.
- ⁴⁴ V. May, O. Kühn, *Charge and Energy Transfer Dynamics in Molecular Systems* Wiley-VCH, Berlin, 2000.
- ⁴⁵ J. A. Leegwater, J. R. Durrant, and D. R. Klug, *J. Phys. Chem. B* **101**, 7205 (1997).
- ⁴⁶ M. Shimizu, S. Suto, and T. Goto, *J. Chem. Phys.* **114** (2001) 2775.
- ⁴⁷ M. Bednarz, V. A. Malyshev, and J. Knoester, *J. Chem. Phys.* **117**, 6200 (2002).
- ⁴⁸ O. Kühn, and V. Sundström, *J. Chem. Phys. B* **107**, 4154 (1997).
- ⁴⁹ T. Renger, V. May, and O. Kühn, *Phys. Rep.* **343**, 137 (2001).
- ⁵⁰ B. Brüggemann, K. Szenee, V. Novoderzhkin, R. van Grondelle, and V. May, *J. Phys. Chem. B* **108**, 13536 (2004).
- ⁵¹ A. V. Malyshev, V. A. Malyshev and F. Domínguez-Adame, *J. Phys. Chem. B* **107**, 4418 (2003).
- ⁵² H. Fidder, J. Knoester, and D. A. Wiersma, *Chem. Phys. Lett.* **171**, 529 (1990).
- ⁵³ I. Renge and U. P. Wild, *J. Phys. Chem. A* **101**, 7977 (1997).
- ⁵⁴ D. J. Heijs, V. A. Malyshev, and J. Knoester, *Phys. Rev. Lett.* **95**, 117402 (2005); *J. Chem. Phys.* **123**, 144507 (2005).
- ⁵⁵ M. Bednarz, V. A. Malyshev, and J. Knoester, *Phys. Rev. Lett.* **91**, 217401 (2003); *J. Chem. Phys.* **120**, 3827 (2004).